nature nanotechnology

ARTICLES

PUBLISHED ONLINE: 21 OCTOBER 2012 | DOI: 10.1038/NNANO.2012.167

The nanomechanical signature of breast cancer

Marija Plodinec[1,2], Marko Loparic[1,2†], Christophe A. Monnier[1†], Ellen C. Obermann[3†], Rosanna Zanetti-Dallenbach[4†], Philipp Oertle[1], Janne T. Hyotyla[1], Ueli Aebi[2], Mohamed Bentires-Alj[5], Roderick Y. H. Lim[1]* and Cora-Ann Schoenenberger[2]

Cancer initiation and progression follow complex molecular and structural changes in the extracellular matrix and cellular architecture of living tissue. However, it remains poorly understood how the transformation from health to malignancy alters the mechanical properties of cells within the tumour microenvironment. Here, we show using an indentation-type atomic force microscope (IT-AFM) that unadulterated human breast biopsies display distinct stiffness profiles. Correlative stiffness maps obtained on normal and benign tissues show uniform stiffness profiles that are characterized by a single distinct peak. In contrast, malignant tissues have a broad distribution resulting from tissue heterogeneity, with a prominent low-stiffness peak representative of cancer cells. Similar findings are seen in specific stages of breast cancer in MMTV-PyMT transgenic mice. Further evidence obtained from the lungs of mice with late-stage tumours shows that migration and metastatic spreading is correlated to the low stiffness of hypoxia-associated cancer cells. Overall, nanomechanical profiling by IT-AFM provides quantitative indicators in the clinical diagnostics of breast cancer with translational significance.

Physical and chemical forces mediate the order by which cells proliferate, differentiate and migrate[1] within the three-dimensional microenvironment of living tissue[2]. Perturbations to this intricate balance[3–5] are known to promote tumorigenesis and progression to metastasis[6]. At the molecular level, tumour initiation and progression are accompanied by complex structural changes in the extracellular matrix (ECM) and cellular architecture, which are anticipated to develop differentiable mechanical responses[7]. However, it has been difficult to reach a consensus as to how such biomechanical heterogeneities occur and what their role might be. This is due to challenges in being able to discriminate between the mechanoresponses of cells and the surrounding ECM within native tumour tissue with adequate spatial/structural resolution and force sensitivity. Not least for its implications in diagnostics and treatment, being able to understand the mechanobiology of tumorigenesis is paramount in revealing its deterministic role in cancer development and metastasis[5].

Long-standing ambiguities exist because efforts to understand cancer biomechanics are largely polarized between tumour-level and single-cell experimentation. In accordance with conventional wisdom (breast palpation), studies on whole mouse mammary glands show that breast tumours are considerably more rigid than the surrounding tissue due to a relative stiffening of the peripheral tumour stroma[7,8]. This notion is consistent with the increase in matrix deposition and crosslinking observed in three-dimensional cell cultures and mouse mammary glands during cancer progression[9,10]. Paradoxically, biophysical techniques[11–16] reveal that single (cultured) cancer cells are more compliant (or 'softer') than their healthy counterparts. This increase in elasticity and/or deformability is accompanied by alterations in the cytoarchitecture that have known associations with malignant transformation[17]. Because of their softness, cancer cells have been detected by indentation-type atomic force microscopy (IT-AFM) in tissue sections from tumours that were surgically removed from patients with advanced cancer[18]. Furthermore, Cross *et al.* found that metastatic cells isolated from the pleural fluid of human patients are softer than normal cells[12], suggesting that metastasis might be promoted by cell compliance. No doubt, criticism is common on both sides of the length-scale divide. On the one hand, the mechanoresponse of whole tumours is arguably dominated by stiff structural elements in the peripheral stroma (for example, collagen[19,20]), leaving potentially more compliant regions in the underlying cancerous core insensitive to detection. On the other hand, the relevance of single cell measurements has been questioned given the lack of a proper three-dimensional tissue environment[21].

The diversity of biomechanical profiles underscores the importance of obtaining a holistic understanding of malignancy and how it manifests in breast tumours. This includes correlating biomechanical and microenvironmental properties at different stages of cancer progression. In this Article, we report on a comprehensive effort to correlate the nanomechanical properties of native human breast biopsies to specific histopathological markers in healthy tissue and in benign and malignant tumours. As a standard animal model, our human biopsy results are validated with systematic experiments on MMTV-PyMT (mouse mammary tumour virus-polyoma middle T antigen) transgenic mice[22], which we follow from early cancer to metastasis. In bridging across length scales, our nanomechanical measurements reconcile tumour-level and single-cell measurements in both humans and transgenic mice and reveal unique mechano-markers that can be used to identify different cancer stages. Moreover, these findings suggest close correlations between cell softening, tumour hypoxia and lung metastasis.

Nanomechanical signatures of human breast biopsies

To elucidate and correlate the respective nanomechanical profiles to pathohistological findings in normal, benign and malignant biopsies, we carried out IT-AFM analyses of *ex vivo* breast tissues under physiological buffer conditions. The experimental approach

[1]Biozentrum and the Swiss Nanoscience Institute, University of Basel, 4056 Basel, Switzerland, [2]Maurice E. Mueller Institute for Structural Biology, Biozentrum, University of Basel, 4056 Basel, Switzerland, [3]Institute of Pathology, University Hospital Basel, 4031 Basel, Switzerland, [4]Department of Gynecology and Gynecological Oncology, University Hospital Basel, University of Basel, 4031 Basel, Switzerland, [5]Mechanisms of Cancer, Friedrich Miescher Institute for Biomedical Research, 4058 Basel, Switzerland; †These authors contributed equally to this work. *e-mail: roderick.lim@unibas.ch

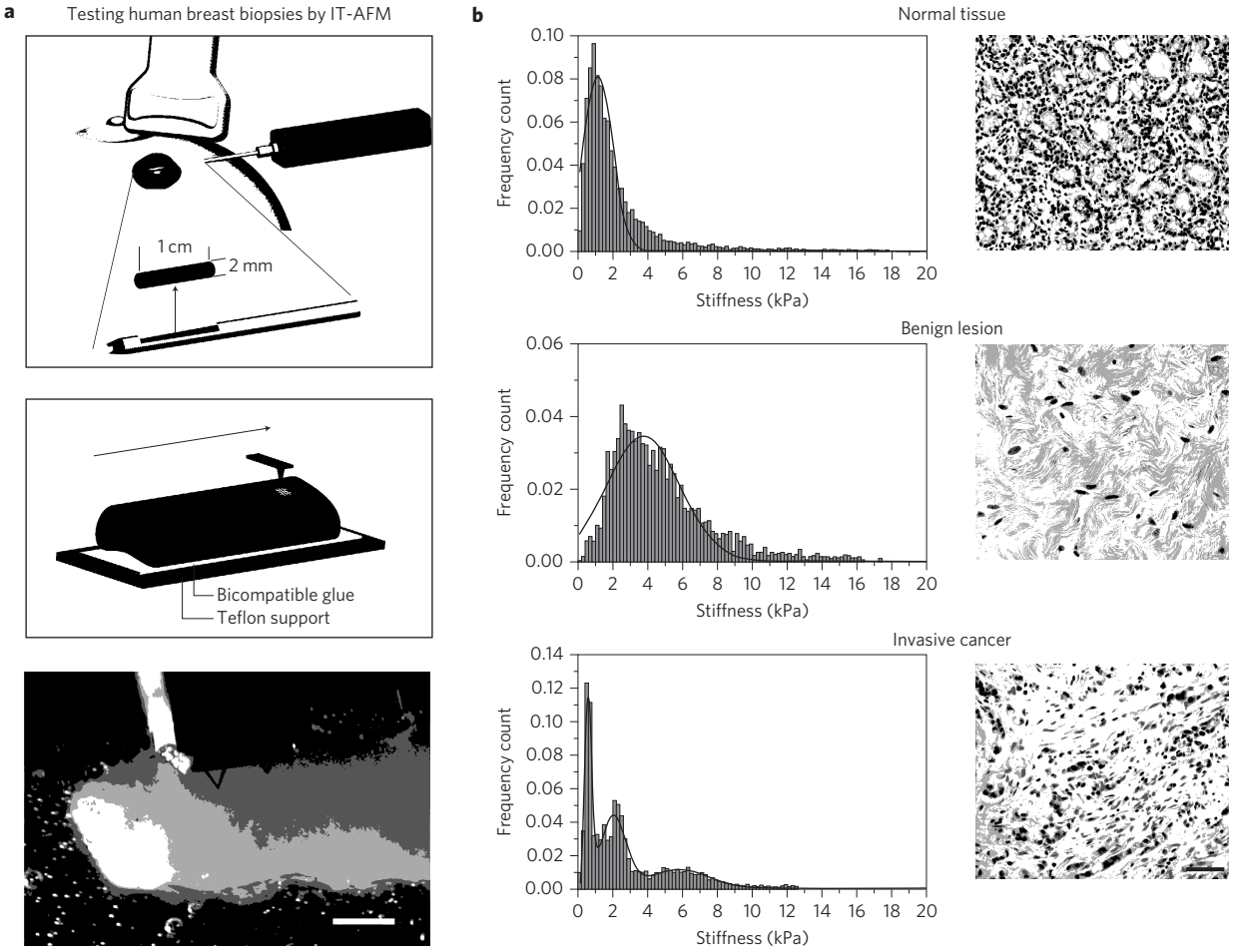

Figure 1 | Nanomechanical signatures of human breast tissue. a, Top: schematic of an ultrasound-guided biopsy from a patient with a suspicious lesion. Middle: multiple stiffness maps (20 × 20 μm each) are recorded in a defined geometrical pattern across the entire specimen. Bottom: top view of an oriented, immobilized biopsy in Ringer's solution with the cantilever positioned for IT-AFM. Scale bar, 500 μm. **b**, Top left: stiffness distribution for normal mammary gland tissue is unimodal. Top right: post-AFM H&E-stained section reveals the terminal ductal lobular unit of a normal mammary gland fenced by interstitial connective tissue. Middle left: biopsy-wide histogram for a benign lesion reveals a unimodal but broader stiffness distribution with an increase in stiffness compared with the healthy biopsy. Middle right: H&E-stained section reveals extensive fibrotic stroma interspersed with fibroblasts typical for fibroadenoma. Bottom left: heterogeneous stiffness distribution with a characteristic soft peak for malignant tumour tissue is consistent with histopathology (bottom right), revealing an invasive breast carcinoma with infiltrating nests of cancer cells that have evoked a dense fibrous tissue response. Scale bar applies to all images, 50 μm.

for obtaining multiple stiffness maps across entire biopsies is described in Fig. 1a. The tissue architecture and surface integrity of the biopsies were confirmed by scanning electron microscopy (SEM; Supplementary Fig. S1). Plotting a histogram of biopsy-wide stiffness values from a healthy specimen reveals a unimodal stiffness distribution of 1.13 ± 0.78 kPa (Fig. 1b, top left). Healthy ducts define the histological appearance in haematoxylin & eosin (H&E)-stained sections of the mapped specimen (Fig. 1b, top right). The benign fibroadenoma with its characteristic highly fibrotic content shows an increased stiffness of 3.68 ± 1.92 kPa (Fig. 1b, middle left). Softer features (<2 kPa) presumably represent individual fibroblasts embedded in the fibrotic stroma. Post-AFM histological examination of the mapped specimen confirmed fibroblasts to be the dominant cell type within the benign lesion[23] (Fig. 1b, middle right).

In comparison, a representative cancer biopsy typically exhibits a bimodal stiffness distribution with two prominent peaks at 0.57 ± 0.16 kPa ('peak 1') and 1.99 ± 0.73 kPa ('peak 2') (Fig. 1b, bottom left). At values stiffer than 2 kPa, a broadening in the distribution indicates a marked mechanical heterogeneity across the sample, with 'peak 3' located at 5.75 ± 1.62 kPa. Post-AFM H&E staining confirmed the dominance of tumour cells that infiltrate the stroma in a cord-like pattern (Fig. 1b, bottom right). We also assigned individual stiffness peaks to specific tissue morphologies by performing more detailed measurements within defined regions of the biopsy (Fig. 2a), in particular in the core (Fig. 2b) and at the periphery (Fig. 2c). The correlation of local AFM data with matching histologies corroborated that the soft peak is typical for cancer cells (Fig. 2b) that are surrounded by stiffer peripheral stroma (Fig. 2c).

Individual biopsy-wide stiffness distributions for 30 human biopsies (8 healthy, 8 benign and 14 malignant) are displayed in Supplementary Fig. S2 and peak stiffness values are summarized in Supplementary Table S1. In general, the nanomechanical signature of healthy breast tissue is characterized by a unimodal distribution with peak stiffness from 1.13 to 1.83 kPa. The stiffness distribution across benign lesions remains uniform; however, stiffness values range from 1.91 to 3.68 kPa and thus indicate a stiffer phenotype. All 14 biopsies with cancer exhibited a characteristic stiffness profile with a dominant peak at 0.31–0.75 kPa, that is, at least factor of two softer than healthy mammary gland epithelium ($P < 0.0001$). The nanomechanical signature of cancer included a second peak between 1.54 and 1.99 kPa. Another feature found in

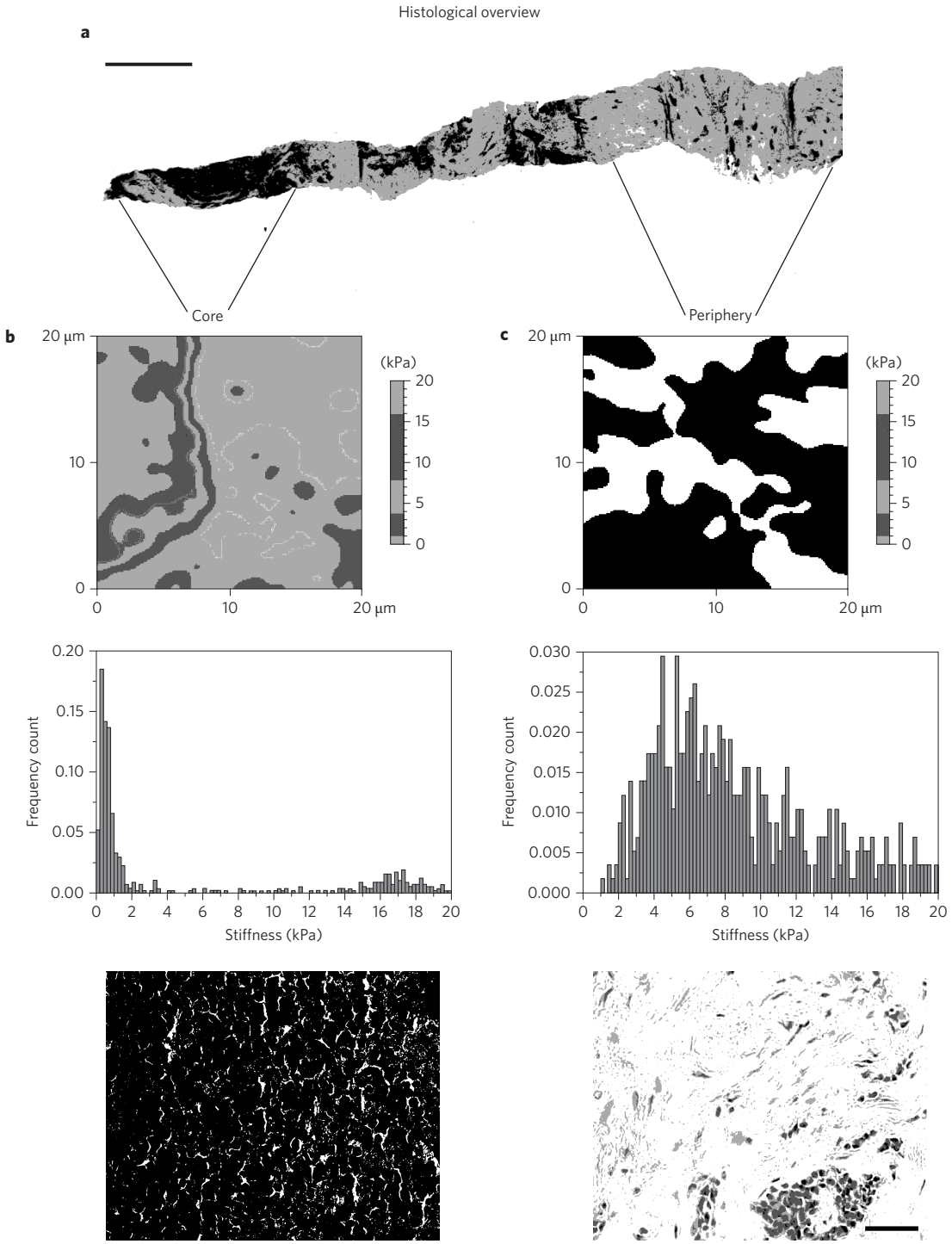

Figure 2 | Stiffness varies from core to periphery in human cancer biopsies. a, Post-AFM histological overview of the entire cancer biopsy with reference to the areas mapped in detail. Scale bar, 500 µm. **b**, Top: representative AFM stiffness map (24 × 24 pixels) of the core region visualizes pronounced softness within a narrow peak of specific stiffness values (middle). Bottom: the local histology shows that the core region is densely populated with cancer cells. **c**, Top: typical stiffness map (24 × 24 pixels) of the tumour periphery demonstrates stiff features. Middle: the corresponding stiffness distribution is broader and shifted towards stiffer values. Bottom: post-AFM histopathology reveals that the tumour periphery predominantly comprises fibrotic tissue. Scale bar, 50 µm (also applies to image in **b**).

several malignant biopsies is that the remaining stiffness values are broadly distributed up to ~20 kPa. This spread is indicative of the overall loss of mammary gland architecture accompanied by tumour vascularization and infiltration, and changes in the invasion-afflicted peripheral ECM[19,24]. Interestingly, cancer biopsies often demonstrate a distinct minimum (~1.1–1.5 kPa, Supplementary Fig. S3) between the primary and secondary peaks. Because it is inversely correlated to the average stiffness value for healthy breast tissue (Supplementary Fig. S3), we interpret the minimum to arise from the malignant transformation of healthy epithelium.

Nanomechanical staging of tumour progression

Because of the genetic and epidemiologic diversity in human patients we turned to MMTV-PyMT transgenic mice, a reliable model for

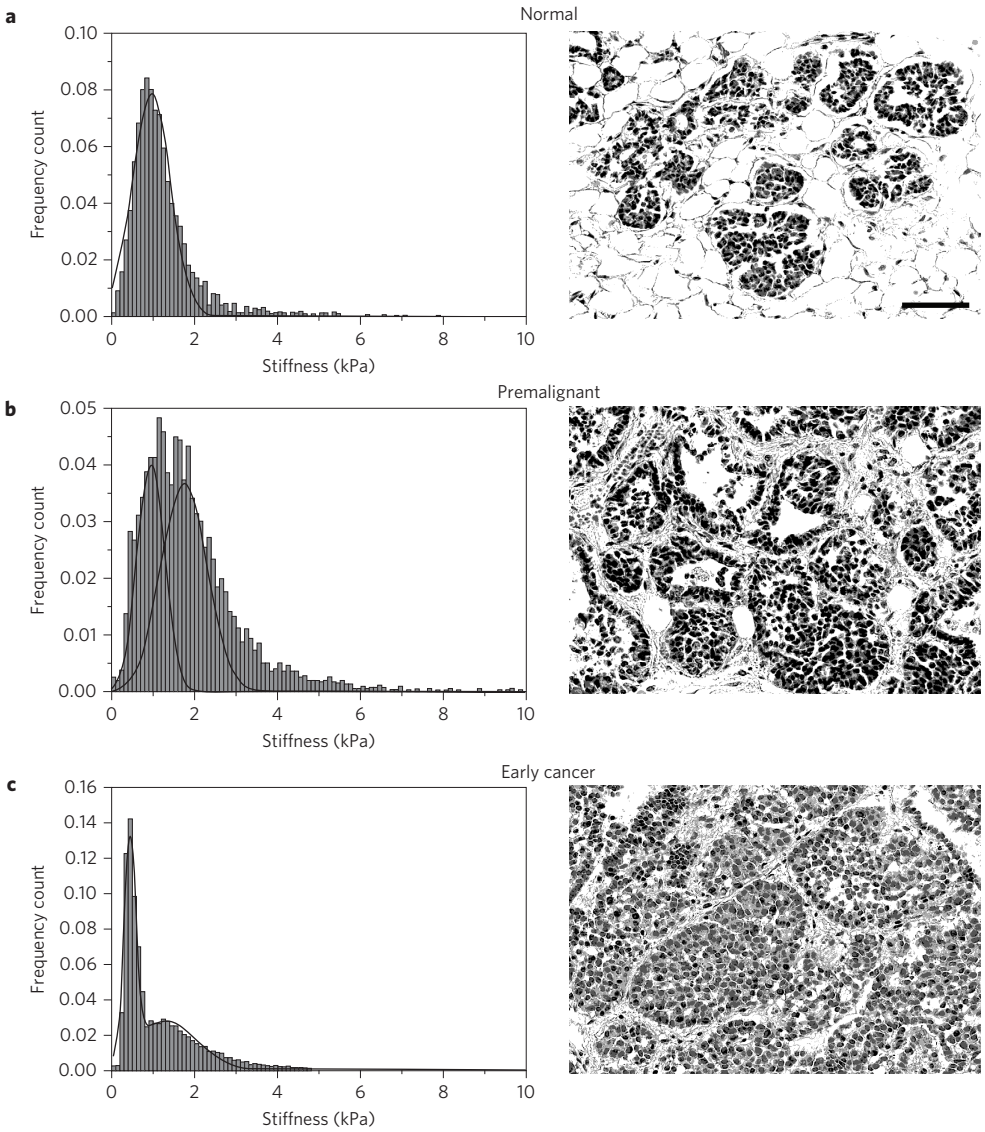

Figure 3 | Correlating the nanomechanical response with tumour progression in MMTV-PyMT mice. a, Left: stiffness values of normal ductal epithelium follow a uniform Gaussian distribution. Right: post-AFM H&E-stained section shows a non-lactating mammary gland with a duct surrounded by adipose tissue. **b**, Left: in the premalignant lesion, the contribution of stiffer features increases, as seen by a broader stiffness distribution with an indication of bimodality. Right: H&E-stained sections of the same tissue show extensive proliferation of epithelial cells and an increase of the surrounding stromal components. **c**, Left: in early cancer, the significant softening produces a characteristic peak that dominates the prominent bimodality of the stiffness distribution. Right: in the H&E section, cancer cells are delineated by stromal tissue. Scale bar in **a** applies to images in **b** and **c**, 50 μm.

human breast cancer, to more systematically elucidate the nanomechanical markers of tumour progression and metastasis[22]. For the corresponding staging of MMTV-PyMT specimens used for stiffness mapping, we monitored the loss of integrin β1 expression, which accompanies tumour progression[22] (Supplementary Fig. S4).

The biopsy-wide histogram across a normal mouse mammary gland revealed a unimodal stiffness distribution with a peak of 1.02 ± 0.42 kPa (Fig. 3a, left) that is characteristic of healthy mammary tissue, with its well-organized arrangement of densely packed epithelial cells (Fig. 3a, right). The uniform stiffness profile is comparable to that of normal human breast. It should be noted, however, that in contrast to human breast tissues, healthy murine mammary glands exhibit extensive amounts of adipose tissue (70–80%) (Supplementary Fig. S5a).

The biopsy-wide histogram of premalignant tissues shows the onset of a bimodal stiffness distribution with peaks at 0.95 ± 0.18 and 1.75 ± 0.27 kPa, as identified by peak-analysing software. The presence of soft and moderately stiffer features correlates with an increase of stromal components surrounding the proliferative cell masses revealed in H&E stained sections (Fig. 3b, right).

In early cancer samples, this trend is more pronounced, resulting from distinct soft and stiff areas (Fig. 3c, left), as demonstrated by the peaks at 0.45 ± 0.12 and 1.29 ± 0.76 kPa, respectively. These correspond to distinct zones of densely packed cancer cells and early stromal invasion, as revealed in H&E stained sections (Fig. 3c, right). A summary of the peak stiffness values that were calculated for murine mammary tissues is presented in Supplementary Table S2.

As mentioned above, adipose tissue is prevalent in murine mammary glands and, because of its softness, could be mistaken for cancer cell clusters. Control experiments on adipose tissues demonstrated that the two cell types could be discriminated by their stiffness (Supplementary Fig. S5). Mammary adipocytes exhibit a stiffness of 0.31 ± 0.13 kPa (Supplementary Fig. S5a, middle), whereas cancer cells have a stiffness peak at 0.75 ± 0.25 kPa (Supplementary Fig. S5b, middle).

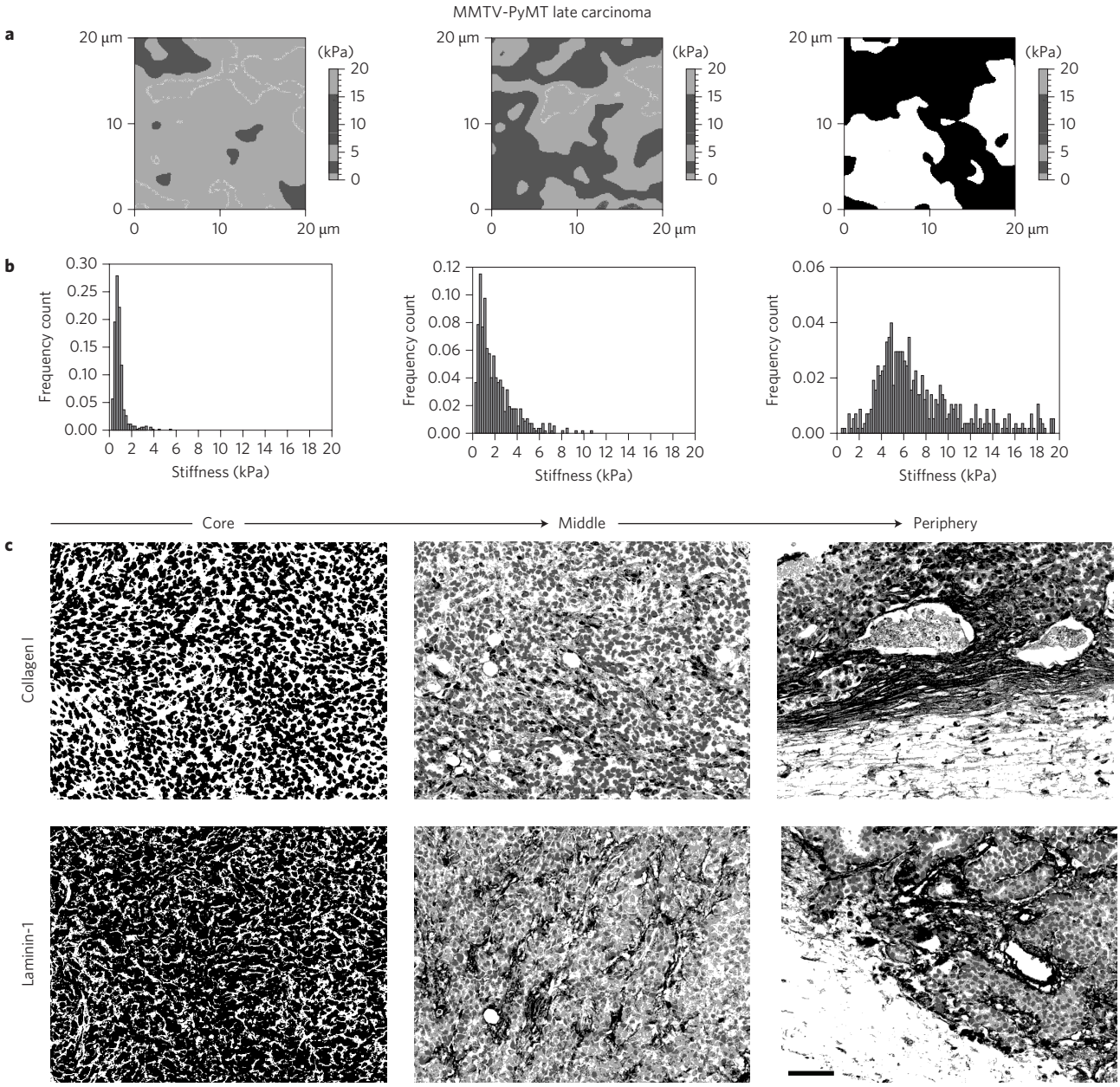

Figure 4 | Correlating local nanomechanical properties and ECM structure in late cancer. a, Consecutive stiffness maps (24 × 24 pixels) across the sample demonstrate a significant increase in stiffness and mechanical heterogeneity from core to periphery (left to right). **b**, Corresponding stiffness distributions change from the core to the periphery. **c**, IHC analysis (brown staining) reveals associated structural and morphological changes in collagen I (top) and laminin-1 (bottom) from core to periphery. Scale bar applies to all images, 50 µm.

Among the most substantial structural changes in mammary gland architecture that occur with the transition from normal mammary gland to early cancer are the degradation of the basement membrane that surrounds normal and premalignant glands (Supplementary Fig. S6, top) and the altered expression and organization of collagen I (Supplementary Fig. S6, bottom). In later stages of tumour progression, stromal contributions increasingly modify cancer behaviour[25]. For example, collagen I, which is the main component of the ECM, is associated with cancer stiffening[19,21]. Therefore, we examined the relation between local nanomechanical profiles and ECM structure in late MMTV-PyMT cancer, which corresponds to invasive ductal carcinomas in humans. Sequential stiffness maps across the specimen demonstrate gradual stiffening from the core to the periphery (Fig. 4a), with peak values shifting from 0.74 ± 0.26 kPa in the core to 5.51 ± 1.70 kPa at the periphery (Fig. 4b). At the same time, mechanical heterogeneity increases and is most extensive at the periphery. These changes appear to be associated with distinct changes in the ECM, as revealed by subsequent immunohistochemistry (IHC) analysis (Fig. 4c).

In particular, collagen I is not detected in the soft core but is increasingly present towards the periphery (Fig. 4c, top). Also, laminin-1 expression is virtually absent from the core (Fig. 4c, bottom left), as expected in advanced cancer where the basement membrane has disintegrated[26]. However, the increased vascularization of the mid and peripheral areas resulted in laminin-1 staining of vessel basement membranes (Fig. 4c, bottom middle and right). We conclude that the absence of laminin-1 and collagen I in the core regions contributes to the soft phenotype of cancer cells. On the other hand, the increased staining of laminin-1 and collagen I towards the periphery marks the increase of stromal invasion related to stiffening in the respective regions. Clearly, IHC analyses show that there is considerable tissue heterogeneity at

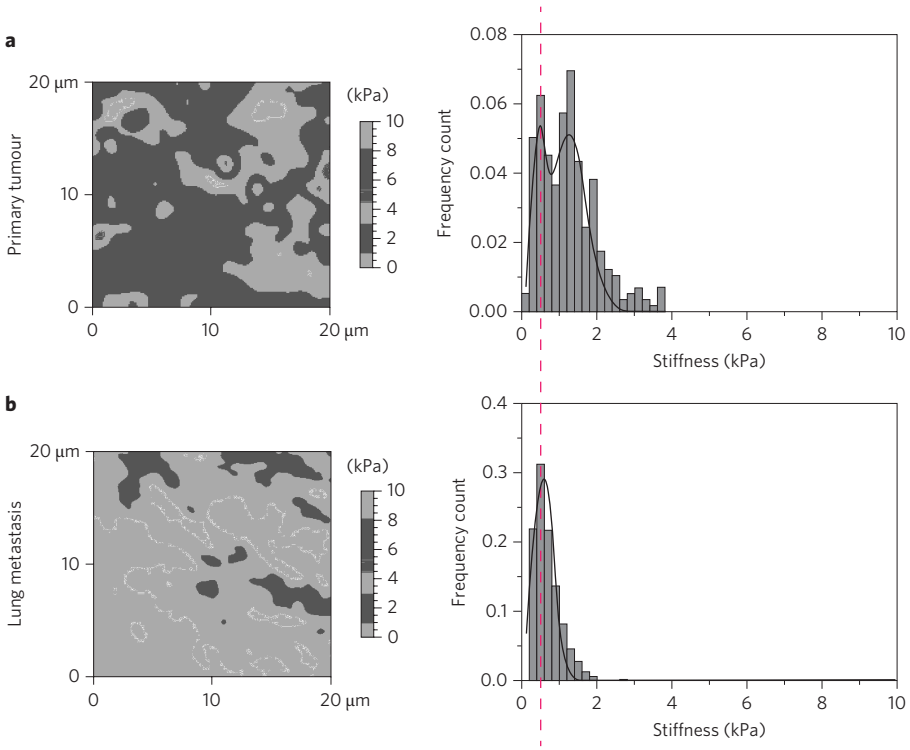

Figure 5 | Stiffness profiles of primary tumour and lung metastasis reveal a common phenotype. a, Left: representative AFM stiffness map (24 × 24 pixels) demonstrates nanomechanical heterogeneity among cancer cells in primary lesions. Right: the corresponding stiffness distribution from the map reveals two peaks representing distinct phenotypes of cancer cells, a softer one at 0.45±0.15 kPa and another at 1.26±0.43 kPa. **b**, Left: representative AFM stiffness map (24 × 24 pixels) of a metastatic lesion and the corresponding stiffness distribution (right) reveal a peak value that is almost identical to the softer peak detected at the primary tumour site (indicated by the red dashed line).

late tumour stages that is reflected in the broad range of stiffness values (Fig. 4b).

The indications that the stiffness signatures are based on distinct changes in the cytoarchitecture and ECM in MMTV-PyMT transgenic mice prompted us to follow up on this correlation in human breast cancer biopsies (Supplementary Fig. S7). Overall, the staining patterns in human biopsies diagnosed with invasive cancer were similar to those observed in the late cancer stage of MMTV-PyMT mammary tissues (Fig. 4, Supplementary Fig. S7). At the cellular level, a distinct expression of desmin and vimentin, both markers of epithelial–mesenchymal transition (EMT), was found in cancer cells, but also in the adjacent stroma of the invasive lobular (Supplementary Fig. S7c) and ductal (Supplementary Fig. S7d) carcinomas. We therefore rationalize that the soft phenotype detected in human cancer biopsies (Supplementary Fig. S2, Table S1) is an indication of tumour progression.

A soft hypoxic cell phenotype is conducive to metastasis

We next asked whether the very soft cancer phenotypes could be associated with the ability to metastasize to distant sites, in particular to the lungs where metastases frequently occur in MMTV-PyMT mice at late stages of tumour progression[27,28]. Stiffness measurements from lungs of mice bearing late-stage tumours reveal an extremely soft peak (Supplementary Fig. S8a) that is absent in healthy lungs (Supplementary Fig. S8b; statistical differences between specimens are presented in Supplementary Table S3). Most importantly, with a stiffness peak of 0.45±0.15 kPa, the softest nanomechanical phenotype present at the primary tumour site (Fig. 5a) closely corresponds to the stiffness of a metastatic lesion obtained from the lungs of the same mouse (0.56±0.26 kPa, Fig. 5b).

Because a hypoxic core is a key feature of aggressive cancers[29], we examined whether the nanomechanical changes associated with cancer progression are related to reduced tumour oxygenation by injecting MMTV-PyMT mice at distinct stages of tumour progression with pimonidazole (a probe that selectively binds to hypoxic cells), 90 min before tumour excision. As expected, normal glands and pre-malignant lesions were negative for hypoxia (Fig. 6, top left and middle). In contrast, early cancer exhibited central hypoxia (Fig. 6, right) that correlated well with a significant decrease of cell stiffness (Fig. 3c, left; Supplementary Table S2). In late cancer, dissemination of hypoxic cancer cells to areas of stromal invasion and to the tumour periphery (Fig. 6, bottom left) adds to the mechanical heterogeneity observed in these regions (Fig. 4b). Moreover, their presence suggests that a decreased stiffness is able to promote the metastatic spread of soft cells to the lungs (Fig. 5).

The role of mechanical properties in cancer development and progression has prompted high-powered research initiatives worldwide. Several studies in recent years have led to the notion that tumours are generally stiffer than healthy tissue[30] and that continuous tissue stiffening is a promoter of cancer[10,31]. Contrary to this dogma, there are numerous studies reporting that single isolated cancer cells are significantly softer than normal cells[32]. However, two-dimensional systems do not recapitulate the architecture or surrounding forces to which a cell is exposed in its native tissue environment[7,33]. Here, our work resolves the stiffness paradox by exploiting the nanomechanical sensitivity of IT-AFM[34] and its unprecedented spatial resolution to comprehensively investigate the mechanical properties of native breast biopsies from human patients (Supplementary Table S1). The most striking finding is that normal glandular tissue, benign lesions and malignant tumours exhibit qualitatively unique biomechanical signatures that are reproducible across different patients. Malignancies are recognized by two features: (i) mechanical heterogeneity in line with histological appearance and (ii) a characteristic stiffness peak of 0.5–0.8 kPa measured in areas with densely packed tumour cells and little intervening stroma. Normal glandular epithelium and benign solid lesions on the other hand each exhibit a

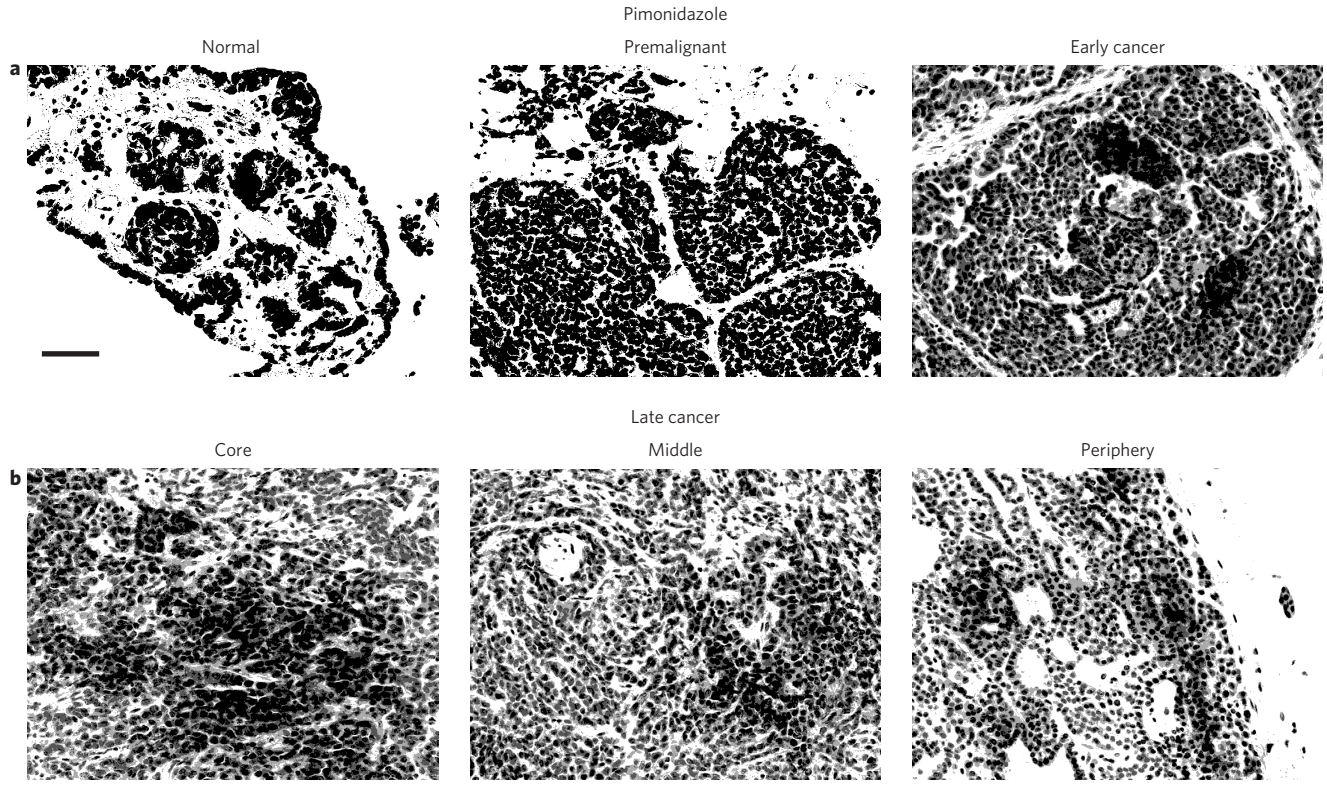

Figure 6 | Dissemination of hypoxic cancer cells increases with tumour progression. Paraffin-embedded sections of mammary gland tissues of pimonidazole (hypoxyprobe)-treated MMTV-PyMT mice at different stages were immunolabelled. **a**, Hypoxia is absent in normal glandular tissue (left) and in premalignant lesions (middle). In contrast, pimonidazole-positive cells (brown staining) reveal central hypoxia in early cancer (right). **b**, In advanced cancer stages, hypoxic cells abundant in the core region (left) are streaming towards tumour blood vessels (middle) and have disseminated to the tumour periphery (right). Scale bar applies to all images, 50 μm.

unimodal stiffness distribution with peaks at ~1 kPa and ~3 kPa, respectively. In fact, signature-based diagnoses in double-blind experiments correlate nearly 100% with conventional histopathology of the same biopsy post-AFM.

Detecting solid breast lesions by differential tissue elasticity is also the underlying principle in sonoelastography, which has emerged as a clinical, non-invasive diagnostic technique in recent years[35]. However, the length scale of this approach does not allow for a reliable distinction of benign and malignant breast masses[36,37]. This challenge is uniquely met by IT-AFM, which is able to differentiate between cancer and benign lesions by correlating stiffness measurements resolved at the nanometre scale across the entire length of a biopsy.

Conclusions

We have resolved the nanomechanical signatures of defined stages of tumour progression, including metastasis. Most notably, high-resolution stiffness mapping has revealed that cancer progression is not limited to matrix stiffening, as previously assumed[10], but is associated with a significant softening of tumour epithelial cells in comparison to normal mammary epithelium. This distinctive softening probably went unnoticed in a recent AFM study[32], because the 5 μm colloidal probe that was used only allowed for bulk measurements that did not provide sufficient resolution to distinguish between the individual tissue components (that is, the cells and ECM[32,38]). Tumour progression to the late, invasive stage accentuates the soft peak and brings about a broadening of the stiffness distribution (Fig. 4) as a result of the cancer cells infiltrating the surrounding tissue, as well as stromal disorganization and tumour vascularization[31].

Recent evidence shows that hypoxia promotes tumour invasion and ultimately metastases, and thus is associated with tumour aggressiveness[38,39]. Also, it has long been hypothesized in the field that metastatic cells need a certain degree of flexibility and deformability to escape their original niche[40–42]. By analysing metastatic lesions in lungs from MMTV-PyMT mice we now provide the first evidence that supports this hypothesis. These data indicate a direct link between cancer cell softening in the primary tumour and aggressive behaviour leading to metastases. In conclusion, soft peaks detected in the primary tumour may serve not only as mechanobiological markers for the onset of cancer but have prognostic qualities as well.

Methods

Human biopsies. Human biopsies were obtained from the outpatient breast clinic, Department of Gynecology and Gynecological Oncology, University Hospital Basel. The study was approved by the institutional review board (ref. no. EK:157/08) and conducted in accordance with ethical guidelines. Patient recruitment was carried out with informed consent. For each patient, one out of five biopsies was used for IT-AFM analysis directly after removal, without previous knowledge of clinical data. The other four biopsies were evaluated by standard pathological procedures. Cylindrical specimens with a diameter of ~0.2 cm and length of 0.2–1 cm were biopsied from suspicious lesions under ultrasound guidance (Fig. 1a). Biopsies were immediately transferred to ice-cold isotonic Ringer solution (6.00 g NaCl, 0.40 g KCl, 50 g anhydric glucose, 0.27 g $CaCl_2$, 3.20 g lactic acid per 1,000 ml of distilled water) supplemented with glucose and a protease inhibitor cocktail (Complete, Boehringer Mannheim; 1 tablet per 10 ml) and kept at 4 °C to minimize tissue degradation. IT-AFM analysis was performed no later than three days after biopsy.

Mammary and lung tissue samples from MMTV-PyMT mice. All procedures involving mice were conducted in accordance with the Swiss laws regulating the use and care of animals in research and have been reviewed and approved by the Federal veterinary office. Female mice heterozygous for the PyMT transgene were obtained by breeding male PyMT mice on a FVB background with FVB females lacking the PyMT transgene. Mice were killed at different time points of tumour development[22], and mammary tissues and lungs from at least six different mice were immediately excised and placed in ice-cold Ringer solution. IT-AFM was performed 1–72 h after tissue removal, after which stiffness profiles were essentially unaltered

(Supplementary Fig. S9) and tissue integrity intact as judged by RNA stability (Supplementary Fig. S9 and Supplementary Information on RNA isolation). For hypoxia assessment, mice were injected intraperitoneally with pimonidazole hydrochloride at 100 mg ml^{-1} in 0.9% sterile saline solution (120 mg kg^{-1}, hypoxyprobe-1, HPI). After 90 min, mice were killed and tissue specimens taken for IT-AFM. Hypoxia was demonstrated by immunohistochemical analysis of pimonidazole incorporation according to a standard protocol[42].

IT-AFM and data analysis. All preparative steps were performed in a sterile buffer environment supplemented with protease inhibitors. Each specimen was immobilized on a plastic dish with a thin layer of two-component fast drying epoxy glue (Devcon). Mechanical manipulations during sample preparation were kept minimal at all times. To level out the surface to be scanned, small wedges were placed under uneven specimens. IT-AFM was carried out with a noise-isolated FlexAFM ARTIDIS (Nanosurf AG) and a Nanowizard I atomic force microscope (JPK Instruments). To compensate for large surface corrugations on such native biological samples, we developed and implemented customized homebuilt hardware and software algorithms for automated levelling, which enabled uninterrupted AFM operation during data acquisition (see Supplementary Information on Automated levelling). A top-down microscope (S8AP0 with Imagesource DFK 31F03, Leica) was used to visually position the AFM cantilever with respect to the specimen. Four-sided pyramidal tips (205-μm-long DNP-S10 triangular silicon nitride cantilevers, resonance frequency (air) $f = 18$ kHz, nominal cantilever spring constant $k = 0.06$ Nm^{-1}, tip radius = 20 nm, half-open angle of the pyramidal face of $\theta \approx 35°$, Bruker) were used. The exact spring constant k of the cantilever was determined before each experiment using the thermal tune method[43] and the deflection sensitivity was determined in fluid using glass substrates as an infinitely stiff reference material. IT-AFM at room temperature involved recording up to 22 different 20 × 20 μm^2 force–volume maps over 24 × 24 point grids (576 force–displacement curves per map and a pixel size of 833 nm) and for high spatial resolution 72 × 72 point grids (5,184 force–displacement curves per map and a pixel size of 277 nm) were recorded. Force–volume maps spaced at 500 μm apart were acquired in a systematic manner across the entire sample surface (Fig. 1a). Individual force curves consisted of 512 data points, with a Z piezo-displacement between 5 and 8 μm, which were collected at 0.8–1 load/unload cycles per second. The maximum applied loading force was set to 1.8 nN, which gave indentation depths that varied approximately between 150 and 3,000 nm depending on the intrinsic mechanical differences within each biopsy (examples are shown in Supplementary Fig. S10). Force curves were analysed using the Oliver and Pharr method[44] as described previously[45–47]. See Supplementary Methods on Oliver and Pharr analysis for further details. The stiffness values (Pa = N m^{-2}) calculated from force curves were spatially plotted to yield colour-coded stiffness maps in Igor Pro 6.22 (Wavemetrics). A two-dimensional spline interpolation was performed on the stiffness maps to smooth the visual presentation of the data.

Statistics. A total of 30 human breast biopsies from female patients (Supplementary Table S1) and 27 mammary glands and 6 lungs obtained from 13 MMTV-PyMT mice were analysed. All individual stiffness values for a specimen were summarized in OriginPro 8.5 (Microcal) to obtain the distribution of stiffness values (henceforth defined as biopsy-wide histogram). The bin width was set to 200 Pa for all mammary gland specimens and 500 Pa for the murine lungs. Counts were normalized according to the total amount of measured stiffness values per specimen. For data fitting, peaks were located with the peak analysis application of OriginPro. Subsequently, a multi-peak fit was applied to the stiffness distribution. All data are given as mean ± standard deviation. The statistical significance of differences in mean values was assessed with the paired Student's t-test in OriginPro 8.5. Statistical significance was set at $P \leq 0.05$.

Immunohistochemical analysis. After IT-AFM, all samples were retrieved, formalin-fixed and paraffin-embedded according to standard histological procedures. Sections with a thickness of ~5 μm were cut and transferred onto coated glass slides. The first and last slides of sequential sections were routinely stained with H&E. Subsequent histopathological examination included assessing the type of lesion (invasive ductal carcinoma, fibroadenoma and so on) and a number of standard histopathological markers (extent of tumour infiltration, fibrosis, necrosis and lymphocytic infiltration). For IHC analysis of the remaining slides of human mammary tissues, the following antibodies were used: anti-collagen I (1:80; Biologo CO2111), anti-laminin (1:25; Thermo RB-082-A, Thermo Scientific), anti-vimentin (prediluted, Ventana 790-2917, Roche Diagnostics), anti-desmin (prediluted, Ventana 760-2513, Roche Diagnostics). IHC analysis of murine tissue sections for laminin was performed in the same manner as for human sections. In addition, murine sections were stained with anti-β1 integrin (1:50, Abcam, ab52971) and anti-mouse collagen I (1:800, Abcam, ab34710). In some cases, sections were treated for antigen retrieval by heat or with 10 mM Tris buffer, 1 mM EDTA, pH 9.0 and citrate buffer, pH 6.0. For collagen staining of human biopsies, sections were pre-treated with pepsin for 30 min at room temperature. Avidin/biotin was used for blocking non-specific binding of the primary antibody. For immunolabelling, sections were incubated with 100 μl antibodies correspondingly diluted in 10 mM PBS, pH 7.6 and 0.1% sodium azide. Staining was visualized with horseradish peroxidase (HRP)-conjugated secondary antibodies (DakoCytomation). Sections were examined with an upright light microscope (Carl Zeiss) at the magnifications indicated.

Received 29 June 2012; accepted 29 August 2012; published online 21 October 2012

References

1. Ingber, D. E. *et al.* Cellular tensegrity—exploring how mechanical changes in the cytoskeleton regulate cell-growth, migration, and tissue pattern during morphogenesis. *Int. Rev. Cytol.* **150,** 173–224 (1994).
2. Park, C. C., Bissell, M. J. & Barcellos-Hoff, M. H. The influence of the microenvironment on the malignant phenotype. *Mol. Med. Today* **6,** 324–329 (2000).
3. Needham, D. Possible role of cell cycle-dependent morphology, geometry, and mechanical-properties in tumor-cell metastasis. *Cell Biophys.* **18,** 99–121 (1991).
4. Paszek, M. J. & Weaver, V. M. The tension mounts: mechanics meets morphogenesis and malignancy. *J. Mammary Gland Biol.* **9,** 325–342 (2004).
5. Kumar, S. & Weaver, V. Mechanics, malignancy, and metastasis: the force journey of a tumor cell. *Cancer Metast. Rev.* **28,** 113–127 (2009).
6. Kass, L., Erler, J. T., Dembo, M. & Weaver, V. M. Mammary epithelial cell: influence of extracellular matrix composition and organization during development and tumorigenesis. *Int. J. Biochem. Cell B* **39,** 1987–1994 (2007).
7. Butcher, D. T., Alliston, T. & Weaver, V. M. A tense situation: forcing tumour progression. *Nature Rev. Cancer* **9,** 108–122 (2009).
8. Sinkus, R. *et al.* High-resolution tensor MR elastography for breast tumour detection. *Phys. Med. Biol.* **45,** 1649–1664 (2000).
9. Paszek, M. J. *et al.* Tensional homeostasis and the malignant phenotype. *Cancer Cell* **8,** 241–254 (2005).
10. Levental, K. R. *et al.* Matrix crosslinking forces tumor progression by enhancing integrin signaling. *Cell* **139,** 891–906 (2009).
11. Rosenbluth, M. J., Lam, W. A. & Fletcher, D. A. Force microscopy of nonadherent cells: a comparison of leukemia cell deformability. *Biophys. J.* **90,** 2994–3003 (2006).
12. Cross, S. E., Jin, Y. S., Rao, J. & Gimzewski, J. K. Nanomechanical analysis of cells from cancer patients. *Nature Nanotech.* **2,** 780–783 (2007).
13. Lekka, M. *et al.* Elasticity of normal and cancerous human bladder cells studied by scanning force microscopy. *Eur. Biophys. J. Biophy.* **28,** 312–316 (1999).
14. Ward, K. A., Li, W. I., Zimmer, S. & Davis, T. Viscoelastic properties of transformed-cells—role in tumor-cell progression and metastasis formation. *Biorheology* **28,** 301–313 (1991).
15. Lam, W. A., Rosenbluth, M. J. & Fletcher, D. A. Chemotherapy exposure increases leukemia cell stiffness. *Blood* **109,** 3505–3508 (2007).
16. Guck, J. *et al.* Optical deformability as an inherent cell marker for testing malignant transformation and metastatic competence. *Biophys. J.* **88,** 3689–3698 (2005).
17. Suresh, S. Biomechanics and biophysics of cancer cells. *Acta Mater.* **55,** 3989–4014 (2007).
18. Lekka, M. *et al.* Cancer cell detection in tissue sections using AFM. *Arch. Biochem. Biophys.* **518,** 151–156 (2012).
19. Weaver, V. M. *et al.* Matrix crosslinking forces tumor progression by enhancing integrin signaling. *Cell* **139,** 891–906 (2009).
20. Erler, J. T. & Weaver, V. M. Three-dimensional context regulation of metastasis. *Clin. Exp. Metastasis* **26,** 35–49 (2009).
21. Weaver, V. M., DuFort, C. C. & Paszek, M. J. Balancing forces: architectural control of mechanotransduction. *Nature Rev. Mol. Cell. Biol.* **12,** 308–319 (2011).
22. Lin, E. Y. *et al.* Progression to malignancy in the polyoma middle T oncoprotein mouse breast cancer model provides a reliable model for human diseases. *Am. J. Pathol.* **163,** 2113–2126 (2003).
23. Lundin, M., Lundin, J., Helin, H. & Isola, J. A digital atlas of breast histopathology: an application of web based virtual microscopy. *J. Clin. Pathol.* **57,** 1288–1291 (2004).
24. Weaver, V. M. *et al.* Tensional homeostasis and the malignant phenotype. *Cancer Cell* **8,** 241–254 (2005).
25. Egeblad, M. & Werb, Z. New functions for the matrix metalloproteinases in cancer progression. *Nature Rev. Cancer* **2,** 161–174 (2002).
26. Albrechtsen, R., Nielsen, M., Wewer, U., Engvall, E. & Ruoslahti, E. Basement membrane changes in breast cancer detected by immunohistochemical staining for laminin. *Cancer Res.* **41,** 5076–5081 (1981).
27. Guy, C. T., Cardiff, R. D. & Muller, W. J. Induction of mammary tumors by expression of polyomavirus middle T oncogene: a transgenic mouse model for metastatic disease. *Mol. Cell Biol.* **12,** 954–961 (1992).
28. Fantozzi, A. & Christofori, G. Mouse models of breast cancer metastasis. *Breast Cancer Res.* **8,** 212 (2006).
29. Guppy, M. The hypoxic core: a possible answer to the cancer paradox. *Biochem. Biophys. Res. Commun.* **299,** 676–680 (2002).
30. Sedwick, C. Valerie Weaver: overcoming cancer's stiff resistance. *J. Cell. Biol.* **193,** 802–803 (2011).
31. Lopez, J. I., Kang, I., You, W. K., McDonald, D. M. & Weaver, V. M. *In situ* force mapping of mammary gland transformation. *Integr. Biol. (Camb.)* **3,** 910–921 (2011).

32. Suresh, S. Biomechanics and biophysics of cancer cells. *Acta Biomater.* **3,** 413–438 (2007).
33. Alcaraz, J. *et al.* Collective epithelial cell invasion overcomes mechanical barriers of collagenous extracellular matrix by a narrow tube-like geometry and MMP14-dependent local softening. *Integr. Biol. (Camb.)* **3,** 1153–1166 (2011).
34. Stolz, M. *et al.* Early detection of aging cartilage and osteoarthritis in mice and patient samples using atomic force microscopy. *Nature Nanotech.* **4,** 186–192 (2009).
35. Thomas, A. *et al.* Real-time elastography—an advanced method of ultrasound: first results in 108 patients with breast lesions. *Ultrasound Obst. Gyn.* **28,** 335–340 (2006).
36. Burnside, E. S. *et al.* Differentiating benign from malignant solid breast masses with US strain imaging. *Radiology* **245,** 401–410 (2007).
37. Xu, H. Y. *et al.* Axial-shear strain imaging for differentiating benign and malignant breast masses. *Ultrasound Med. Biol.* **36,** 1813–1824 (2010).
38. Wong, C. C. L. *et al.* Hypoxia-inducible factor 1 is a master regulator of breast cancer metastatic niche formation. *Proc. Natl Acad. Sci. USA* **108,** 16369–16374 (2011).
39. Erler, J. T. *et al.* Lysyl oxidase is essential for hypoxia-induced metastasis. *Nature* **440,** 1222–1226 (2006).
40. Fritsch, A. *et al.* Are biomechanical changes necessary for tumour progression? *Nature Phys.* **6,** 730–732 (2010).
41. Wirtz, D., Konstantopoulos, K. & Searson, P. C. The physics of cancer: the role of physical interactions and mechanical forces in metastasis. *Nature Rev. Cancer* **11,** 512–522 (2011).
42. Erler, J. T., Jeffrey, S. S. & Giaccia, A. J. Hypoxia promotes invasion and metastasis of breast cancer cells by increasing lysyl oxidase expression. *Breast Cancer Res.* **7,** S57 (2005).
43. Sader, J. E., Larson, I., Mulvaney, P. & White, L. R. Method for the calibration of atomic-force microscope cantilevers. *Rev. Sci. Instrum.* **66,** 3789–3798 (1995).
44. Oliver, W. C. & Pharr, G. M. An improved technique for determining hardness and elastic-modulus using load and displacement sensing indentation experiments. *J. Mater. Res.* **7,** 1564–1583 (1992).
45. Plodinec, M., Loparic, M. & Aebi, U. Atomic force microscopy for biological imaging and mechanical testing across length scales. *Cold Spring Harb. Protoc.* **2010,** pdb top86 (2010).
46. Loparic, M. *et al.* Micro- and nanomechanical analysis of articular cartilage by indentation-type atomic force microscopy: validation with a gel-microfiber composite. *Biophys. J.* **98,** 2731–2740 (2010).
47. Plodinec, M. *et al.* The nanomechanical properties of rat fibroblasts are modulated by interfering with the vimentin intermediate filament system. *J. Struct. Biol.* **174,** 476–484 (2011).

Acknowledgements

The authors thank U. Mueller for excising tissues from MMTV-PyMT mice, T. Nguyen and P. Hirschmann for technical assistance with histology and IHC, and R. Suetterlin for advice on IHC. B. Bircher is acknowledged for his contribution to AFM data analysis, T. Pfändler for logistic support concerning clinical samples and A. Roulier for help with the drawing in Fig. 1. The authors also thank U. Sauder for SEM sample preparation, D. Mathys for SEM imaging and P. Demougin for RNA extraction. This work is funded by the National Centre of Competence in Research 'Nanoscale Science', Swiss National Science Foundation (to C-A.S.), and the Commission for Technology and Innovation (CTI) supporting university–industry partnerships (Project 11977.2 PFNM-NM within the project ARTIDIS 'Automated and Reliable Tissue Diagnostics' awarded to R.Y.H.L in partnership with Nanosurf AG). R.Z.D. is supported by Krebsliga Beider Basel (grant no. 22-2010). The laboratory of M.B-A. is supported by the Novartis Research Foundation, the European Research Council (ERC starting grant no. 243211-PTPsBDC), the Swiss Cancer League and the Krebsliga Beider Basel.

Author contributions

M.P., R.Y.H.L. and C-A.S. conceived the study and designed experiments. M.P., M.L. and R.Y.H.L. developed all customized hardware and software solutions for AFM. M.P. and E.C.O. performed pathohistological and IHC analysis of human and murine tissues. R.Z.D. recruited patients and provided human biopsies. M.P., C.A.M. and P.O. performed AFM experiments. M.P., M.L, C.A.M., J.T.H., P.O. and R.Y.H.L. analysed AFM data. M.B-A. provided MMTV-PyMT mice and was involved in the analysis of murine tissues. M.P., U.A., R.Y.H.L. and C-A.S. wrote the paper. All authors discussed the results and commented on the manuscript.

Additional information

Supplementary information is available in the online version of the paper. Reprints and permission information is available online at http://www.nature.com/reprints. Correspondence and requests for materials should be addressed to R.Y.H.L.

Competing financial interests

The University of Basel has filed patents on the technology and intellectual property related to this work based on the inventions of M.P., M.L. and R.Y.H.L.